Journal of Applied Electrochemistry (2007) 37:415–420
DOI 10.1007/s10800-006-9272-2

TiO_2-mediated photoelectrochemical decoloration of methylene blue in the presence of peroxodisulfate

E. VALATKA* and Ž. KULĖŠIUS
*Department of Physical Chemistry, Kaunas University of Technology, Radvilenu st. 19, LT-50254, Kaunas, Lithuania (*author for correspondence, tel.: +370-37-300167, fax: +370-37-300152, e-mail: evalatka@ktu.lt)*

Received 10 July 2006; accepted in revised form 20 October 2006

Key words: methylene blue, photocurrent, photoelectrochemical, stainless steel, titanium dioxide

Abstract

Nanosized TiO_2 films on stainless steel were prepared by electrophoretic deposition and characterized by X-ray diffraction analysis and photo-voltammetry. The decoloration of methylene blue (MB) dye was used as a test reaction for the evaluation of photoelectrocatalytic activity of the prepared TiO_2 coatings. The influence of applied potential and potassium peroxodisulfate on the rate of MB decoloration was investigated. The possible mechanisms of MB oxidation under various experimental conditions are discussed.

1. Introduction

Recently, particular attention has been paid to the photocatalytic properties of titanium dioxide (TiO_2) which is widely used in the production of dyes, pharmaceuticals, cosmetics [1]. It has been shown that TiO_2 can be used as an efficient photocatalyst for the oxidation of organic and inorganic compounds [2–7], water photosplitting to hydrogen and oxygen [8] and manufacture of photoelectrochemical cells [9]. Nanocrystalline TiO_2 in the anatase form appears to be the most photoactive and the most practical of the semiconductors for these purposes. Much work has focused on photochemical activity using suspensions of powdered TiO_2, but for practical use it is an advantage to use immobilized catalyst. TiO_2 films on various types of substrate can be synthesized using sol–gel, hydrothermal synthesis, spray-pyrolysis, dip-coating and chemical vapor deposition methods [10]. However, the main drawbacks of the use of supported TiO_2 photocatalyst are small total surface area and mass transport limitations. In order to increase its efficiency, TiO_2 can be deposited on electroconductive substrate and biased positively by applying an external voltage. In such a photoelectrochemical system, the rate of photoelectron and hole recombination is reduced; consequently, the rate of surface reactions is increased (so called electrically enhanced photocatalysis). Electrically conductive supports can be covered with TiO_2 by using electrophoresis. Electrophoretic deposition (EPD) is a well-known method which is widely used for synthesis of ceramic layers from aqueous or non-aqueous powder suspensions. The main advantages of EPD are as follows [11, 12]: possibility of coating formation of controlled thickness on complex shapes, low cost process requiring simple equipment and reliability.

The aim of this work was to prepare TiO_2 coatings on stainless steel using EPD and to study the photoelectrochemical activity of TiO_2 electrodes in the presence of methylene blue (MB) dye as a model pollutant. This work is relevant to the development of photochemical methods for the oxidative destruction of organic pollutants such as textile dyes. These compounds are not readily degraded by conventional treatment methods (biological, ozonation, chlorination). Therefore, there is a great need to find a more efficient method which could be partly or entirely driven by solar radiation.

2. Experimental

2.1. *Preparation of nanoparticulate TiO_2 electrodes*

TiO_2 coatings on stainless steel were prepared by using EPD. Commercially available TiO_2 powder (Degussa P25) was used as a starting material due to its well-documented photoactivity and known physical properties (~80% of anatase, ~20% of rutile, small amount of amorphous phase, specific surface area ~50 $m^2\ g^{-1}$, particle size ~20 nm [13]). AISI 304 stainless steel plates 0.5 mm thick were used as a support.

A suspension for EPD was prepared by dispersing TiO_2 (2 g) into 100 ml of methanol (purity 99.5%, Lachema, Czech Republic). Homogeneous suspension was achieved under vigorous stirring for 30 min. Two stainless steel plates (5 cm × 2.5 cm each) were

immersed into a prepared suspension of TiO_2. The distance between anode and cathode was 1.5 cm. EPD synthesis was performed under constant voltage (30 V) and was controlled using a DC power supply B5-49 (MNIPI Inc., Russia). The deposition time was varied from 5 to 30 s. In order to obtain better adhesion of TiO_2, all samples were thermally treated under air atmosphere in a 300–450 °C range for 1 h.

2.2. *Analytical techniques*

The electrochemical measurements in the dark and under UV illumination were performed by computer-controlled Autolab PGSTAT12 (Ecochemie, The Netherlands) potentiostat/galvanostat. The GPES® 4.9 software was used for the collection and treatment of experimental data. A two-compartment photoelectrochemical quartz cell was employed. The electrolyte volume in each compartment was the same (100 ml). The anodic compartment contained the TiO_2 working electrode and Ag, AgCl|KCl(sat) reference electrode. The cathodic compartment held a platinum wire (geometric area about 15 cm^2) as a counter electrode. Voltammograms were run for at least three consecutive cycles since preliminary experiments showed that a near-steady state response was observed only after the second run. All results correspond to the stabilized voltammetric behavior. 0.1 M K_2SO_4 (purity > 99%, Reachim, Russia) solution was used as a supporting electrolyte. The back side of the TiO_2 electrode was insulated with epoxy resin in order to eliminate its contribution to the dark current. The coated area of electrode was carefully positioned under UV irradiation. A General Electric F8W/BLB lamp (λ_{max} = 366 nm) was placed at a distance of 2 cm from the TiO_2 electrode and was used as UV radiation source. The incident light intensity was evaluated by potassium ferrioxalate actinometry [14]. The average power density at 366 nm was calculated to be 1.8 mW cm^{-2}.

The photoelectrocatalytic activity of the prepared TiO_2 films was tested in the decoloration reaction of methylene blue dye ($C_{16}H_{18}N_3SCl \cdot 3H_2O$, purity > 99%, Reachim, Russia). All solutions were prepared with doubly distilled water and were not deaerated during experimental runs. All measurements were carried out at ambient temperature (291 K).

The same experimental set-up and conditions (solution volume, electrodes, UV radiation source) were used both in photovoltammetry and bulk photoelectrolysis experiments. The only difference was that during bulk photoelectrolysis the solution was thoroughly stirred.

An UV–vis spectrophotometer Perkin-Elmer Lambda 25 was used for the determination of methylene blue concentration by measuring the absorbance at λ_{max} = 660 nm.

The X-ray powder diffraction (XRD) data were collected with DRON-6 (Bourevestnik Inc., Russia) powder diffractometer with Bragg–Brentano geometry using Ni-filtered Cu K_α radiation and graphite monochromator. The rutile content in the TiO_2 electrode was calculated from the equation [15]:

$$x = \left(1 + 0.8\frac{I_A}{I_R}\right)^{-1},$$

where x is the weight fraction of rutile in the powders and I_A and I_R are the intensities of the characteristic peaks of anatase and rutile, respectively.

The crystallite sizes of anatase and rutile were calculated from line broadening by using the Scherrer equation [16]:

$$D_{hkl} = \frac{k\,\lambda}{B_{hkl}\cos\Theta},$$

where λ is the wavelength of the Cu K_α radiation (1.54056×10^{-10} m), θ the Bragg diffraction angle, B_{hkl} the full width at half maximum intensity of the anatase (2θ = 25.3°) and rutile (2θ = 27.5°) reflection peaks and k a constant (the value used in this study was 0.94).

3. Results and discussion

3.1. *Structural characterization of TiO_2 electrodes*

The amount of TiO_2 deposited on stainless steel is dependant on the electrophoresis time (Figure 1). The rate of TiO_2 film formation is 0.045 mg cm^{-2} s^{-1}, as calculated from the slope. The most uniform and mechanically stable TiO_2 films were obtained when deposition time was in the range 10–15 s. Under such conditions, the amount of TiO_2 deposited is 0.5–0.7 mg cm^{-2}. Assuming that the bulk density of P25 TiO_2 is 3.8 g cm^{-3} [17], the approximate thickness of these TiO_2 coatings is 1.32–1.84 μm.

The XRD pattern of the P25 TiO_2 powder on AISI 304 stainless steel reveals the characteristic peaks of anatase (101) and rutile (110) at 2θ = 25.4° and 27.5°, respectively (Figure 2). On the basis of these peak intensities, the rutile content in the TiO_2 electrode was calculated to be 27.08%.

The crystallite sizes of anatase and rutile were calculated according to the Scherrer equation. The

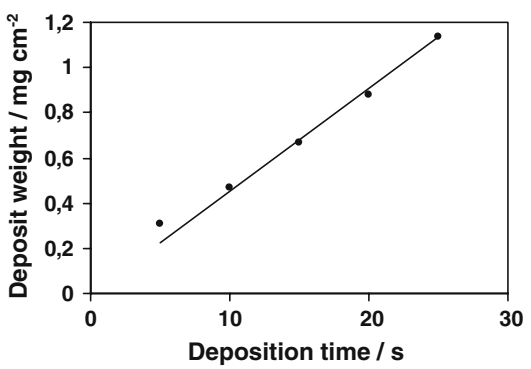

Fig. 1. The amount of immobilized TiO_2 as a function of electrophoretic deposition time at 30 V.

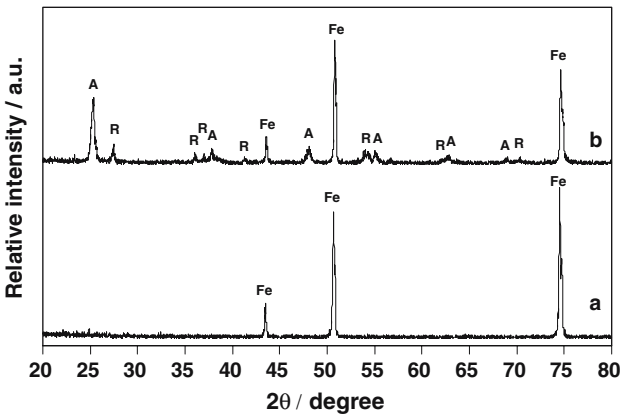

Fig. 2. XRD patterns of pure AISI 304 stainless steel (a) and TiO_2 (b) electrodes annealed at 400 °C for 1 h. Indexes: A – anatase, R – rutile, Fe – iron.

calculated values of crystallite sizes are 20.8 nm (anatase) and 53.5 nm (rutile).

3.2. *Photoelectrochemical characterization of TiO_2 coatings*

3.2.1. *Photoelectrochemical behavior in supporting electrolyte*

Figure 3 shows characteristic voltammograms of a TiO_2 electrode in 0.1 M K_2SO_4 solution. The potential was swept from −0.2 to +1.0 V at 10 mV s^{-1}. The photoelectrochemical behavior of polycrystalline TiO_2 electrodes was determined from current–potential curves obtained both in the dark and under UV irradiation. The difference between the dark and light currents is the photocurrent. The anodic photocurrent observed on nanocrystalline n-type TiO_2 electrode is due to the diffusion of photogenerated electrons through the particulate film to the counter electrode [18]. The observed photocurrent can be related to the generation of $OH^{\bullet}$ radicals and other oxidation products ($O_2^{\bullet -}$, $HO_2^{\bullet}$, H_2O_2) at the surface of the TiO_2 electrode [2]. At higher than +0.4 V potentials the photocurrent reaches a limiting value. This limiting photocurrent is a measure of the overall photo(electro)catalytic efficiency of the TiO_2 electrode and is influenced by various factors (catalyst structure, particle size and form, electrode conductivity, etc.). The observed increase in current at higher than +0.8 V potentials is associated with the transpassive dissolution of stainless steel and oxygen evolution [19]. The inset in Figure 3 shows a plot of the square of photocurrent against applied potential. This plot is expected to be linear if the semiconductor layer is thick enough for the development of a space charge layer [18]. However, in our case no linearity is observed and the photocharacteristics cannot be interpolated by a Gartner–Butler equation [18, 20]. This means that the space charge layer for the prepared P25 TiO_2 electrode is not formed and charge separation occurs via diffusion. In contrast, when single-crystal or polycrystalline material is used, the space charge layer is formed at the electrode/electrolyte interface. This space charge layer facilitates the separation of photogenerated holes and electrons. However, in the case of nanoparticulate films the space charge layer is not formed because the individual particles in the film are very small. In such small particles the charge recombination is still a dominant process. So, application of an anodic bias to the TiO_2 nanoparticulate electrode provides the possibility of separating charge carriers and to minimize charge recombination.

The value of photocurrent depends on the electrode heat treatment temperature (Figure 4). The highest photocurrent density (15.3 μA cm^{-2}) was obtained with an electrode annealed at 400 °C for 1 h. In such a case, the incident photon-to-current efficiency (IPCE) was estimated to be 2.88%. The IPCE value of a photoelectrode was calculated using the expression [21]:

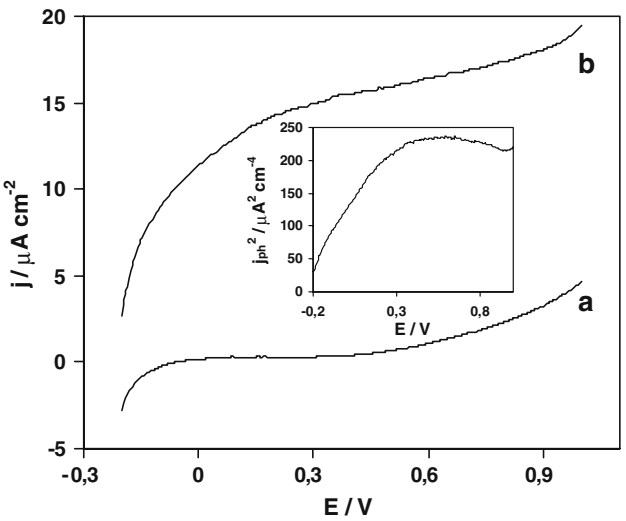

Fig. 3. Characteristic voltammograms of TiO_2 electrode in 0.1 M K_2SO_4 solution at 18 °C in the dark (a) and under UV illumination (b) recorded at a 10 mV s^{-1} potential scan rate. Inset: dependence of j_{ph}^2 on applied potential.

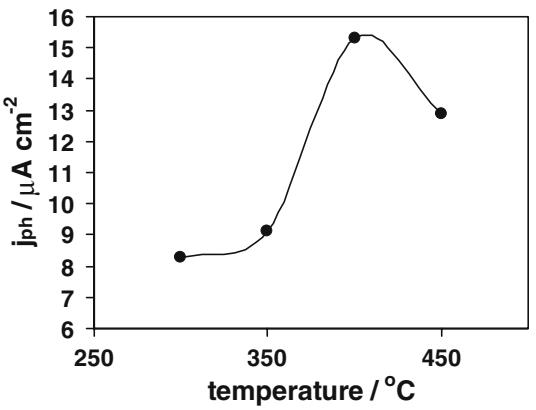

Fig. 4. The dependence of the photocurrent density j_{ph} at +0.6 V in 0.1 M K_2SO_4 supporting electrolyte at 18 °C on thermal treatment temperature of TiO_2 electrode.

$$\mathrm{IPCE}(\%) = 100\frac{1240 j_{ph}}{\lambda P},$$

where j_{ph} is the photocurrent in mA cm^{-2}, λ the wavelength of the incident light in nanometers and P is the incident light intensity in mW cm^{-2}.

Taking into account the results presented in Figures 1 and 4, in all subsequent experimental runs we used the TiO_2 electrode prepared under the following conditions: annealing temperature 400 °C, TiO_2 amount 0.5 mg cm^{-2}.

3.2.2. *Photoelectrochemical behavior in the presence of methylene blue*

Figure 5 shows current–potential curves for TiO_2 electrodes in 0.1 M K_2SO_4 supporting electrolyte in the presence of methylene blue at various concentrations. The potential was swept from −0.2 to +0.6 V at a 10 mV s^{-1}.

In the dark, the anodic currents were negligible both in the absence and presence of MB (curve a). The photocurrents increased steeply with the potential bias at low potentials and then saturated at more positive potentials (curves b–f). This can be explained by assuming that at low potentials the electron transport in the film controls the overall photocatalytic process; thus, the photocurrent increases with potential [18]. Once the rate of electron transport inside the film reaches a level comparable to the rate of photohole capture at the TiO_2/solution interface, the photocurrent is saturated. Under such conditions the overall reaction is controlled by the photohole capture at the interface. The photocurrent reflects the rate of photohole capture at the TiO_2 interface, which is determined by the availability of electron donors (for instance, organic compounds) at the TiO_2 surface, their interaction with the surface, the nature of their intermediates and the molecular steric suitability of adsorbed form of organic compounds to capture photoholes [21–23].

The data presented in Figure 5 show that photocurrent decreases with MB concentration. A similar dependence of photocurrent on initial solute concentration was observed in the case of phthalic and salicylic acids [22], which are known to be strongly adsorbed onto titania. The authors suggested that the decrease in photocurrent can be related to the accumulation of aromatic intermediates at the electrode surface. These intermediates can act as photohole/photoelectron recombination centers and reduce the overall efficiency of the photocatalytic processes.

It is known that various intermediate compounds are formed during methylene blue oxidation [24–26]. These compounds can interact differently with the TiO_2 surface and markedly influence the processes of photohole capture.

3.2.3. *Effect of applied bias and peroxodisulfate ($S_2O_8^{2-}$) ions on MB decoloration rate*

In a photoelectrochemical system, photoelectrons and holes are separated under the influence of an applied electric field and the efficiency of the photodegradation process can be significantly improved. This is confirmed experimentally by studying the influence of applied bias on the MB decoloration rate (Figure 6). The rate increases upon application of an external potential from 0.0 to 1.0 V (curves e–g) as compared to pure photocatalysis (curve d). At potentials +0.8 and +1.0 V, pure electrochemical oxidation without UV irradiation was observed (curves b and c). No decrease in MB concentration was detected at potentials below +0.6 V in the dark (curve a). However, despite the fact that the rate of MB decoloration significantly increases at potentials higher than +0.8 V both in the dark and under UV irradiation, the transpassive dissolution of stainless steel must be taken into account [19]. From a practical point of view, the transpassive dissolution is an important issue as the photoelectrocatalytic activity of TiO_2 electrode can diminish over prolonged operation time. The photostability of a TiO_2 electrode during organic degradation is currently under investigation and the results will be published separately.

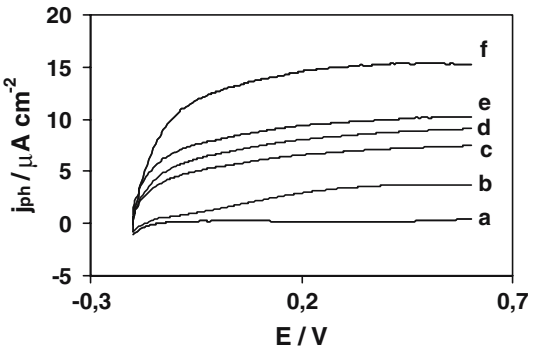

Fig. 5. Voltammograms of TiO_2 film electrode in 0.1 M K_2SO_4 solution at 10 mV s^{-1} potential scan rate and 18 °C under UV illumination at different methylene blue (MB) concentrations: (a) 1.40×10^{-5} M in the dark; (b) 1.40×10^{-5} M; (c) 2.81×10^{-6} M; (d) 5.62×10^{-7} M; (e) 2.81×10^{-7} M; (f) no MB under UV illumination.

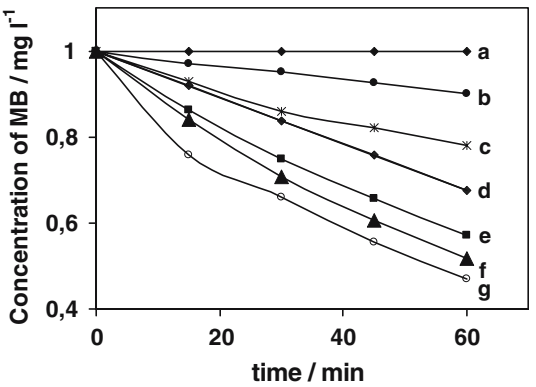

Fig. 6. Influence of applied potential on the rate of MB decoloration at 18 °C under UV irradiation: (a) +0.6 V in the dark; (b) +0.8 V in the dark; (c) +1.0 V in the dark; (d) photocatalysis without applied bias; (e) 0.0 V; (f) +0.6 V; (g) +1.0 V.

Another approach to enhance the rate of photocatalytic oxidation is the use of various oxidants, for instance, peroxodisulfate, hydrogen peroxide or ozone. The use of peroxodisulfates ($S_2O_8^{2-}$) is particularly attractive due to the possibility of regenerating the expended oxidant [27]. The regeneration process involves the oxidation of sulfate ions in acidic medium at a Pt-based anode at 15–30 °C. The rate limiting step in the oxidation of organics using peroxodisulfates is the formation of sulfate ($SO_4^{\bullet -}$) radicals, which are highly reactive species similar to $OH^{\bullet}$. Sulfate radicals are created by the decomposition of peroxodisulfate by thermal activation, UV photolysis or various one-electron reductants [28].

The results presented in Figure 7 show the influence of potassium peroxodisulfate on the rate of MB decoloration. In the absence of UV irradiation, the reaction between MB and peroxodisulfate does not proceed at 18 °C (curve a). Under UV light, the presence of peroxodisulfate significantly increases the rate of MB photocatalytic oxidation without applied bias (curves b and c). The presence of peroxodisulfate at 1.85×10^{-3} M has almost the same effect as an application of external bias of +0.6 V without peroxodisulfate (curves c and d). MB oxidation in the presence of $S_2O_8^{2-}$ ions is further increased when +0.6 V potential is applied (curve e). However, at higher peroxodisulfate concentrations, the influence of applied bias becomes insignificant (curves g and h).

According to the general principles of photocatalysis [2, 3], the enhancement of the photocatalytic oxidation rate by peroxodisulfate can be explained by the simultaneous generation of highly reactive $OH^{\bullet}$ and $SO_4^{\bullet -}$ radicals. When TiO_2 semiconductor is illuminated with radiation shorter than 420 nm, the formation of conduction-band electrons (e_{CB}^-) and valence-band holes (h_{VB}^+) takes place:

$$TiO_2 + h\nu \rightarrow e_{CB}^- + h_{VB}^+ \quad (1)$$

The photoelectrons act as reducing agents for adsorbed species; therefore, their reaction with adsorbed oxygen and/or peroxodisulfate is thermodynamically highly probable:

$$O_2 + e_{CB}^- \rightarrow O_2^{\bullet -} \quad (2)$$

$$S_2O_8^{2-} + e_{CB}^- \rightarrow SO_4^{\bullet -} + SO_4^{2-} \quad (3)$$

The $O_2^{\bullet -}$ radical (reaction 2) may become a source of other oxidizing species, such as hydrogen peroxide, $HO_2^{\bullet}$ and $OH^{\bullet}$ radicals [2]. It is assumed that reaction (3) is the main source of sulfate radicals. It has been established that the photochemical decomposition of peroxodisulfate is highly accelerated in the presence of TiO_2 as compared to pure photolysis in the aqueous phase [29].

The photogenerated holes have a high positive oxidation potential and are able to oxidize water and most organic compounds:

$$H_2O + h_{VB}^+ \rightarrow OH^{\bullet} + H^+ \quad (4)$$

$OH^{\bullet}$ radicals are believed to be the main oxidizing species in photocatalysis. However, when peroxodisulfate is present in reaction solution, reaction (3) can take place generating sulfate radicals. These radicals enter in the reaction chain leading to the enhanced oxidation of organic compounds. Under our experimental conditions it can be assumed that MB degradation is mainly due to the reaction with $OH^{\bullet}$ and $SO_4^{\bullet -}$ radicals:

$$MB + SO_4^{\bullet -} \rightarrow \text{products} \quad (5)$$

$$MB + OH^{\bullet} \rightarrow \text{products} \quad (6)$$

Therefore, the presence of peroxodisulfate ions improves separation of photogenerated electrons and holes and, consequently, increases the overall efficiency of the photocatalytic process. It has been established [25] that the initial step of MB photocatalytic oxidation is the cleavage of the bonds of the $C–S^+=C$ functional group leading to the formation of sulfoxide. Carbon dioxide, nitrate, sulfate and ammonium ions were also identified as reaction products, indicating that the complete oxidation of MB dye can be achieved [25, 26, 30, 31]. In our work the MB mineralization process was not studied.

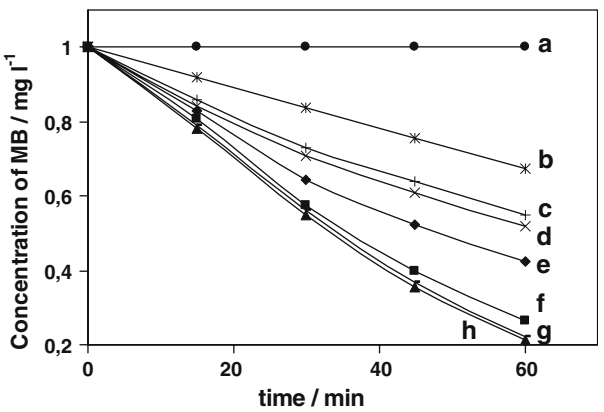

Fig. 7. Effect of $K_2S_2O_8$ concentration on MB decoloration rate under UV irradiation at 18 °C: (a) 5.56×10^{-3} M in the dark without applied bias; (b) photocatalysis without $K_2S_2O_8$ and applied bias; (c) 1.85×10^{-3} M without applied bias; (d) without $K_2S_2O_8$ at +0.6 V; (e) 1.85×10^{-3} M at +0.6 V; (f) 3.7×10^{-3} M at +0.6 V; (g) 5.56×10^{-3} M at +0.6 V; (h) 5.56×10^{-3} M without applied bias.

4. Conclusions

Nanocrystalline P25 TiO_2 films on AISI 304 stainless steel were prepared by EPD. The TiO_2 film is photoactive and the highest photocurrent in 0.1 M K_2SO_4 supporting electrolyte was obtained with the electrode prepared under the following conditions: annealing temperature 400 °C and TiO_2 amount 0.5 mg cm^{-2}. Its photoelectrochemical behavior in the presence of methylene blue dye was studied. It was established that photocurrent decreases as the concentration of MB increases.

The rate of MB decoloration on a TiO_2/stainless steel electrode under UV irradiation increases with increasing positive external voltage and/or potassium peroxodisulfate concentration. However, the experimental results show that the influence of an applied bias of $+0.6$ V becomes insignificant when the concentration of peroxodisulfate is higher than 1.85×10^{-3} M.

References

1. J. Winkler, *Titanium Dioxide* (Vincentz, Hannover, 2003) 128 pp.
2. A.L. Linsebigler, G. Lu and J.T. Yates, *Chem. Rev.* **95** (1995) 735.
3. M.R. Hoffmann, S.T. Martin, W. Choi and D.W. Bahnemann, *Chem. Rev.* **95** (1995) 69.
4. J. Peral, D.X. Xavier and D.F. Ollis, *J. Chem. Technol. Biotechnol.* **75** (1997) 117.
5. D.S. Bhatkhande, V.G. Pangarkar and A. Beenackers, *J. Chem. Technol. Biotechnol.* **77** (2001) 102.
6. A. Fujishima, T.N. Rao and D.A. Tryk, *J. Photochem. Photobiol. C: Chem. Rev.* **1** (2001) 1.
7. K. Kabra, R. Chaudhary and R.L. Sawhney, *Ind. Eng. Chem. Res.* **43** (2004) 7683.
8. T. Bak, J. Nowotny, M. Rekas and C.C. Sorrell, *Int. J. Hydrogen Energ.* **27** (2002) 991.
9. M. Grätzel, *J. Photochem. Photobiol. C: Chem. Rev.* **4** (2003) 145.
10. J.A. Byrne, B.R. Eggins, N.M.D. Brown, B. McKinney and M. Rouse, *Appl. Catal. B.* **17** (1998) 25.
11. A.R. Boccaccini and I. Zhitomirsky, *Curr. Opin. Solid State Mater. Sci.* **6** (2002) 251.
12. R. Moreno and B. Ferrari, *Am. Ceram. Soc. Bull.* **79** (2000) 44.
13. R.I. Bickley, T. Gonzales-Carreno, J.S. Lees, L. Palmisano and R.J.D. Tilley, *J. Solid State Chem.* **92** (1991) 178.
14. J.G. Calvert and J.G. Pitts Jr, *Photochemistry* (Wiley, New York, 1966) 899 pp.
15. R.A. Spurr and H. Myers, *Anal. Chem.* **29** (1957) 760.
16. L.V. Azaroff, *Elements of X-ray Crystallography* (McGraw-Hill Book Co., New York, 1968), 202 pp.
17. Pigments. Highly dispersed metallic oxides produced by the AEROSIL process (Degussa Technical Bulletin N. 56, 1984).
18. K. Rajeshwar, in A.J. Bard, M. Stratmann and S. Licht (eds.) *Encyclopedia of Electrochemistry*, Vol. 6 (Wiley-VCH, 2002) pp. 3–53.
19. I. Betova, M. Bojinov, T. Laitinen, K. Makela, P. Pohjanne and T. Saario, *Corros. Sci.* **44** (2002) 2675.
20. W.W. Gartner, *Phys. Rev.* **116** (1959) 84.
21. I. Mintsouli, N. Philippidis, I. Poulios and S. Sotiropoulos, *J. Appl. Electrochem.* **36** (2006) 463.
22. D. Jiang, H. Zhao, S. Zhang and R. John, *J. Photochem. Photobiol. A: Chem.* **177** (2006) 253.
23. J. Georgieva, S. Armyanov, E. Valova, I. Poulios and S. Sotiropoulos, *Electrochim. Acta* **51** (2006) 2076.
24. H. Gnaser, M.R. Savina, W.F. Calaway, C.E. Tripa, I.V. Veryovkin and M.J. Pellin, *Int. J. Mass Spectrom.* **245** (2005) 61.
25. A. Houas, L. Lachheb, M. Ksibi, E. Elaloui, C. Guillard and J.M. Herrmann, *Appl. Catal. B.* **31** (2001) 145.
26. S. Lakshmi, R. Renganathan and S. Fujita, *J. Photochem. Photobiol. A: Chem.* **88** (1995) 163.
27. P. Kleinschmit, B. Bertsch-Frank, T. Lehmann and P. Panster. *in* B. Elvers, S. Hawkins and G. Schulz (Eds), Ullmann's Encyclopedia of Industrial Chemistry A19, (VCH Verlagsgeselschaft, Weinheim, 1991), pp. 177–197.
28. A.A. Berlin, V.N. Kislenko, *Persulfate Oxidation of Organic Compounds* (Svit, L'vov, 1991) 140 pp. (in Russian).
29. E. Valatka, Phenol Destructive Oxidation: Kinetics and Technological Aspects, *Dissertation*, University of Technology, Kaunas (2000) (in Lithuanian).
30. C. Guillard, H. Lachheb, A. Houas, M. Ksibi, E. Elaloui and J.M. Herrmann, *J. Photochem. Photobiol. A: Chem.* **158** (2003) 27.
31. H. Lachheb, E. Puzenat, A. Houas, M. Ksibi, E. Elaloui, C. Guillard and J.M. Herrmann, *Appl. Catal. B.* **39** (2002) 75.